Chapter 7

Making vancomycin a potent broad-spectrum antimicrobial agent using PEI-stabilized gold nanoparticles as a delivery vehicle

7.1 Introduction

Microbes, including bacteria, viruses, fungi, and parasites, cause human infections. These microbes usually respond well to antimicrobial agents. However, in the present era, emerging drug resistance among *Candida* species and Gram-negative bacteria is a significant concern in healthcare. These drug-resistant microbial infections lead to high mortality rates and expensive medical costs for hospitalized patients (Nami et al., 2018; Medici et al., 2015). *Candida* species associated high mortality rates are due to the frequent occurrence of invasive systemic infections and cases of septicemia, especially in immunocompromised patients (Nami et al., 2018; Medici et al., 2015; Sakagami et al., 2019). *Candida* species, viz. *Candida albicans*, *Candida glabrata*, *Candida tropicalis*, *Candida parapsilosis*, and *Candida krusei*, reside opportunistically in healthy hosts and cause invasive infections when an individual becomes immunocompromised (Spampinato & Leonardi 2013). Despite the availability of antifungal drugs for *Candida* infections, mortality rates continue to be high at 45% (Cheng et al., 2005). Due to general and long-term use, *Candida* resistance has shown an increase in antifungal drugs such as azoles (Nirkhiwale et al., 2014). In addition to *Candida* species, gram-negative bacteria like *E. coli* and *P. aeruginosa* also cause life-threatening human infections. WHO (World Health Organization) estimated 4.95 million deaths associated with AMR bacteria in 2019, mainly driven by six leading pathogens called the ESKAPE group (*Escherichia coli, Staphylococcus aureus, Klebsiella pneumoniae, Streptococcus pneumoniae, Acinetobacter baumannii*, and *Pseudomonas aeruginosa*) (Collaborators, 2022). The rapid emergence of multidrug resistance (MDR) in Gram-negative bacteria poses a significant threat to public

health (Davies et al., 2013; Laxminarayan et al., 2016). The so-called "superbugs" resistant to almost all current antibiotics are frequently isolated from clinics, leaving few therapeutic options available to handle the most complex cases.

Nanotechnology offers a strategic platform that has the potential to counter communicable and non-communicable diseases in a targeted way by using nanoparticles as drug carriers. The physicochemical properties of nanoparticles, such as shape, size, and surface chemistry, are easy to manipulate, making them versatile weapons in fighting bacterial and fungal infections (Hagbani et al., 2022; Rizvi et al., 2023). In addition, due to their high drug-loading efficiency and ability to cross biological membranes, selectively surface-tuned nanoparticles represent excellent antimicrobial drug carriers at the site of infection (Mitchell et al., 2021; Blanco et al., 2015). Several metal nanoparticles and their oxides, such as gold, silver, zinc oxide, copper oxide, aluminum oxide, and titanium dioxide nanoparticles, are rigorously being evaluated, alone or conjugated with antibiotics or other functional molecules, for their potential to treat bacterial and fungal infections (Shabatina et al., 2022; Khorsandi et al., 2021; Kotrange et al., 2021; Klębowski et al., 2018). Among them, gold nanoparticles (Ag-NPs) have attracted significant attention because of their biocompatibility, optical properties, and easy-to-surface tuning with chosen drug molecules (Monti et al., 2019). Recent works endorsed utilizing Au-NPs as drug carriers for antimicrobial agents (Wang et al., 2018; Nawaz et al., 2021; Huang et al., 2023; Park et al., 2022; Rad et al., 2018; Yeom et al., 2016). Due to the sizeable volume-surface ratio, Au-NPs have high drug loading capacity and can efficiently deliver relatively high drug concentrations at the site of infection. For example, Mu et al. demonstrated that combinations of Ag@Au core cell NPs loaded with ciprofloxacin enhance antibacterial activity against *E. coli* (Mu et al., 2021).

Similarly, Shaker et al. (2017) evaluated the surface conjugation of carbapenem (imipenem and Meropenem) with gold nanoparticles as a delivering strategy against *Klebsiella pneumoniae*, *Proteus mirabilis*, and *Acinetobacter baumannii*. The obtained gold nanoparticles showed a distinct nano-size with loading efficiency up to 72% and 74% for Ipm and Mem. Further, the Ipm-loaded gold nanoparticles demonstrated a decrease in the MIC of Ipm down to four folds. In contrast, loaded gold nanoparticles showed a reduction in the MIC of Mem down to three folds on the tested bacterial isolates (Shaker et al., 2017). Some other studies have been conducted to increase the effectiveness of antibacterial drugs by loading AuNPs against bacterial pathogens. For example, Hagbani et al., 2022 used vancomycin-functionalized gold nanoparticles (V-GNPs) to defeat pathogenic bacterial infections. However, the synthesis has taken place in 48 hours at 60^0C. The loading efficiency of vancomycin onto V-GNPs has been demonstrated to be 86.2%. The antibacterial activities of V-GNPs were 1.4-, 1.6-, 1.8-, and 1.6-fold higher against Gram-negative *Escherichia coli*, *Klebsiella oxytoca*, and *Pseudomonas aeruginosa*, and Gram-positive *Staphylococcus aureus*, respectively, compared to pure vancomycin (Hagbani et al., 2022). Similarly, approaches were made to counter antifungal drug resistance against fungal strains by conjugating drugs or small molecules to enhance the killing efficiency of the drug. For example, the anti-candida effects of indolicidin were investigated as a representative of host defense peptide conjugated with gold nanoparticles against fluconazole-resistant clinical isolates of *C. albicans* (Rahimi et al., 2019).

This chapter describes the synthesis-enhanced in vitro antimicrobial activity of water-soluble vancomycin functionalized gold nanoparticles against *Candida* spp. and Gram-negative bacteria *E. coli* and *P. aeruginosa*. Vancomycin is a well-known antibiotic for treating Gram-positive bacterial infections in ICU patients. Chemically, vancomycin is a unique glycopeptide structurally unrelated to any currently available antibiotic. It also has a unique mode of action,

inhibiting the second stage of cell wall synthesis in susceptible bacteria. Since the inter-domain exploration of the antifungal activity of classical antibacterial drugs was neglected. Hence, the approach was to stabilize gold nanoparticles with Polyethyleneimine, a cationic polymer classically used to deliver nucleic acids and genes to mammalian cells, and vancomycin as a payload. Therefore, the current work is opening a window to counter antimicrobial drug resistance by inverting classical antibacterial agents into broad-spectrum agents through delivery at a directed location with Nano carriers' help.

7.2 Experimental Section

7.2.1. Materials

All materials and reagents were of analytical quality. Vancomycin, Polyethyleneimine, chloroauric acid tri hydrate, Amphotericin B, and Meropenem were purchased from Sigma Aldrich, Mumbai, India. For microbial culture, SDA (Sabouraud dextrose agar) and RPMI (Roswell Park Memorial Institute, Buffalo, NY, USA), MHA and MHB were purchased from Hi-Media Laboratories Limited (Mumbai, Maharashtra, India). The other used solvents were purchased from Merck Life Science Private Limited (Bangalore, Karnataka, India). Other required glassware and plastic wares were purchased from Tarson Products Private Limited (Kolkata, West Bengal, India). All the experiments were performed in ultra-purified HPLC-grade water.

7.2.2 Microbial Strains

The ATCC strain of *C. albicans, C. tropicalis, E. coli,* and *P. aeruginosa* were used in this study. The microbial strains were identified by conventional microbiological procedures, including cultural and morphological characteristics, and pure strains were sub-cultured on MHA and stored at -20^{0}C for further experiments.

7.2.3 Synthesis and Characterization of Vancomycin Functionalized Gold Nanoparticles

The PEI-AuNP@Van synthesized and characterized as described in Chapter 6. This chapter is an extended application of PEI-AuNP@Van nanoparticles.

7.2.4 Antimicrobial susceptibility assessment of PEI-AuNP@Van.

The antimicrobial activity of PEI-AuNP@Van was assessed against ATCC strains of *C. albicans, C. tropicalis, E. coli,* and *P. aeruginosa* as per previous guidelines (Ferraro, 2000). Briefly, the log phase grown culture of aforementioned microbial strains (10^7 cfu/ml bacteria and 10^5 cfu/ml fungus) was swabbed on freshly prepared Muller Hinton Agar plates using a sterile cotton swab, followed by drying for 10 min. A wide mouth of clean micropipette tips cut the agar wells, pouring Amphotericin B/Meropenem (positive control), DW (negative control), and PEI-AuNP@Van. The plates were left for 20 min to diffuse properly under sterile conditions and incubated in a static position for 48 h at 37^0C. The experiment was performed in triplicate and mean inhibition zone diameters were measured in millimeters and interpreted following CLSI guidelines, 2019.

7.2.5 Minimal Inhibitory Concentration (MIC) Determination

The minimum inhibitory concentration (MIC) of PEI-AuNP@Van against ATCC strains of *C. albicans, C. tropicalis, E. coli,* and *P. aeruginosa* was determined by applying serial dilution method in a sterile, 96-well, flat-bottom microtiter plate as described previously (MA, 2006). An aqueous suspension of 50 µg/mL PEI-AuNP@Van was prepared, followed by dispensing (100 µl) in the first well and diluted serially; the final concentration was between 0.38 and 50 µg/mL. Similarly, the positive control (Amphotericin B and Meropenem; 32 µg/mL) and negative control (distilled water) were diluted serially. Subsequently, 100 µL of the freshly prepared microbial cultures were added to each well. The microtiter plate was then incubated

in a static position at 37 °C for 24 h; a visual demonstration of turbidity (i.e., a visually clear well) was concluded as the MIC. After that, a 10-µL aliquot from each well was sub-cultured on the MHA/SD agar plates for 24 h; microbial growth was subsequently observed. The MIC data were determined as the concentration of PEI-AuNP@Van at which the development was inhibited or slowed compared to the standard control.

7.2.6 Microbial Growth Reduction Analysis

We used UV-Vis spectrophotometry to track how PEI-AuNP@Van affected the growth rates of the respective microbial strains as previously described (Muloiwa et al., 2020). In summary, overnight-grown microbial strains were allowed to grow to their early exponential phase in fresh MHB broth. Once accomplished, the microbe-containing broth was inoculated into a tissue culture plate with an initial absorbance of 0.01 at a wavelength of max 600 nm. After 2 h, each well's change in absorbance was assessed to evaluate the effects of the intervention.

$$\text{Log reduction} = \log 10(N0/N)$$

Where: N0 = colony forming units of the microorganisms before treatment, N = colony forming units of the microorganisms after treatment with PEI-AuNP@Van.

7.2.7 Super-resolution confocal Laser Scanning Microscopy studies

The PEI-AuNP@Van exposed *C. albicans, C. tropicalis, E. coli*, and *P. aeruginosa* cells viability were assessed using membrane-impermeable dye, propidium iodide (PI) and visualized under super-resolution laser scanning Microscopy. Briefly, freshly grown microbial cells were washed in PBS and suspended in MHB, followed by the addition of PEI-AuNP@Van at their respective MIC along with positive and negative controls in a separated tube and incubated for 4 h at 37^0 C. Further, aliquots were taken from each tube and centrifuged at 3500 rpm for 5 min. The obtained pellet was washed twice with PBS, followed by re-

suspension in PBS. The cells were stained with 10µl (1mg/ml stock) of PI (excitation/emission at 535/617nm), incubated at room temperature under dark conditions for 30 min, followed by washing with PBS to eliminate any excess dye. Subsequently, the treated cells were observed under an SP5 AOBS Super-resolution confocal laser-scanning microscope (Leica, Wetzlar, Germany) with a 40x Immersion oil objective. The antimicrobial activity of PEI-AuNP@Van was concluded by the fact that dead (damaged cell membrane) cells stained with PI and live cells remained unstained since an intact plasma membrane prevents the internalization of PI inside the cell.

7.2.8 Fluorescence Activated Cell Sorting (FACs)

To determine the percentage of dead cells of each microbial strain after 4 h of exposure with PEI-AuNP@Van, a freshly grown culture of *C. albicans*, *C. tropicalis*, *E. coli*, and *P. aeruginosa* was prepared as described above. A 5 ml culture was taken (10^8 cfu/ml of bacterial and 10^6 cfu/ml of fungus, respectively) in MHB/RPMI medium, followed by adding PEI-AuNP@Van at their respective MIC in separate tubes. Further, tubes were incubated at 37^0C for 4 h. After incubation, 2 ml aliquots were pelleted at 3500 rpm for 5 min, followed by washing with PBS. The PEI-AuNP@Van exposed cells were stained with PI (10µl; 1mg/ml) and incubated at room temperature for 30 min under dark conditions. Stained cells were washed with PBS to eliminate any excess stains. Data acquisition was performed with BD Accuri C6 Flow cytometer and BD Accuri C6 software based on light-scatter and fluorescence signals from 20 mW laser illumination at 488 nm. All the measurements were performed logarithmically. The assay was performed at a low sample rate (14-µl min^{-1}). 10^4 events were taken in the case of fungus, while 10^6 were considered for bacterial samples.

7.2.9 Endogenous Reactive Oxygen Species (ROS) Generation Study

PEI-AuNP@Van exposed C. *albicans, C. tropicalis, E. coli*, and *P. aeruginosa* cells were evaluated for Endogenous reactive oxygen species (ROS) production after the exposure for 4 h, monitored by flow cytometry using 2′, 7′-dichlorofluorescein-diacetate (DCFH-DA) as ROS marker as described earlier (Yadav et al., 2020). Freshly grown cultures were exposed at respective MIC followed by washing with PBS, then cell density was adjusted to $10^8/10^6$ cfu/ml for bacteria and fungus. The cell suspensions were incubated for 30 min with 5 µM DCFH-DA, followed by the analysis of ROS accumulation on a BD Accuri C6 Flow cytometer. The data acquisition was performed with BD Accuri C6 software based on light-scatter and fluorescence signals from 20 mW laser illumination at 488 nm. All the measurements were performed logarithmically. The assay was performed at a low sample rate (14-µl min^{-1}). 10^4 events were taken in the case of fungus, while 10^6 were considered for bacterial samples.

7. 2.10 Phosphatidylserine Externalization Studies (Apoptosis assay)

C. albicans, C. tropicalis, E. coli, and *P. aeruginosa* cells were stained with Annexin V-FITC and propidium iodide (PI) (Yadav et al., 2020) with the FITC-Annexin V apoptosis detection kit (BD Pharmingen). *C. albicans, C. tropicalis, E. coli*, and *P. aeruginosa* cells were incubated with PEI-AuNP@Van at the MIC for 4 h at 37 °C and incubated for 20 min in an Annexin V binding buffer containing 5 µl/ml of Annexin V-FITC and 2 µl/ml of PI along with untreated control. Cells were visualized SP5 AOBS Super-resolution confocal laser-scanning microscope (Leica, Wetzlar, Germany) with a 40X Immersion oil objective.

7.2.11 Raman Spectroscopy Studies

The Raman Spectroscopy has been performed to investigate any bimolecular changes in microbial cells after exposure with PEI-AuNP@Van, untreated, and Amphotericin B/Meropenem against *C. albicans, C. tropicalis, E. coli*, and *P. aeruginosa* cells. The PEI-

AuNP@Van, untreated, and Amphotericin B/Meropenem exposed cells were pelleted and washed twice with PBS to remove debris. Then, placed on a microscopic glass slide and dried for 30 min under ambient conditions. Raman measurements were performed using WI Tec alpha 300 RA/S Instrument (WI Tec, GmbH, Germany). The Excitation source for the study was a 532 nm Nd: YAG laser and the maximum power output of the laser was 40 mW. The Laser power was attenuated to ~ 16 mW at the sampling point. The dispersed intensity of light of the signal from the grating was measured by a Peltier-cooled charge-coupled device (CCD), and the spectrum was recorded in the window of 400-2400 cm^{-1}.

7.2.12 TEM characterization of PEI-AuNP@Van treated microbial strains.

For TEM characterization, freshly harvested cells of *C. albicans*, *C. tropicalis*, *E. coli*, and *P. aeruginosa* were prepared and treated with PEI-AuNP@Van at their respective MIC and incubated for 4 h at 37^0C. After exposure, the culture was pelleted down, washed with PB, and fixed with Karnowski solution for 1 h. Further, control and treated samples were drops cast on a carbon-coated copper grid having a mess size of 300 and dried under ambient conditions for 1 h. The visualization has been done through FEI TECHNAI G2 20 S TWIN TEM.

7.3 Results

7.3.1 Synthesis and characterization of PEI-AuNP@Van nanoparticles

The results of the synthesis and characterization of vancomycin-functionalized gold nanoparticles are discussed in Chapter 6.

7.3.2 In-vitro antimicrobial activity of PEI-AuNP@Van nanoparticles

The antimicrobial activity of PEI-AuNP@Van evaluated by Agar well diffusion method and MIC were determined by broth micro-dilution against *C. albicans*, *C. tropicalis*, *E. coli*, and *P. aeruginosa* along with positive and negative controls. The results demonstrated that PEI-

AuNP@Van had excellent antimicrobial activity against *Candida* species and gram-negative *E. coli* and *P. aeruginosa*. The zone of inhibition against *C. tropicalis* (24 mm) was high as compared to *C. albicans* (14 mm), *E. coli* (20 mm), and *P. aeruginosa* (17 mm), as shown in Figure 7.1 (a-e). These results confirmed the high sensitivity of *C. tropicalis* and *P. aeruginosa* for PEI-AuNP@Van compared to *C. albicans* and *E. coli*. The constant zone of inhibition until 72 h of incubation agrees with the biocidal action of PEI-AuNP@Van against all treated strains.

Minimum inhibitory concentration (MIC) of PEI-AuNP@Van, determined against *C. albicans*, *C. tropicalis*, *E. coli*, and *P. aeruginosa* by broth micro-dilution method. The MIC of PEI-AuNP@Van against *C. albicans* (4.8 µg/ml), *C. tropicalis* (1.2 µg/ml), *E. coli* (2.5 µg/ml), and *P. aeruginosa* (4.81 µg/ml) respectively as depicted in Figure 7.2.

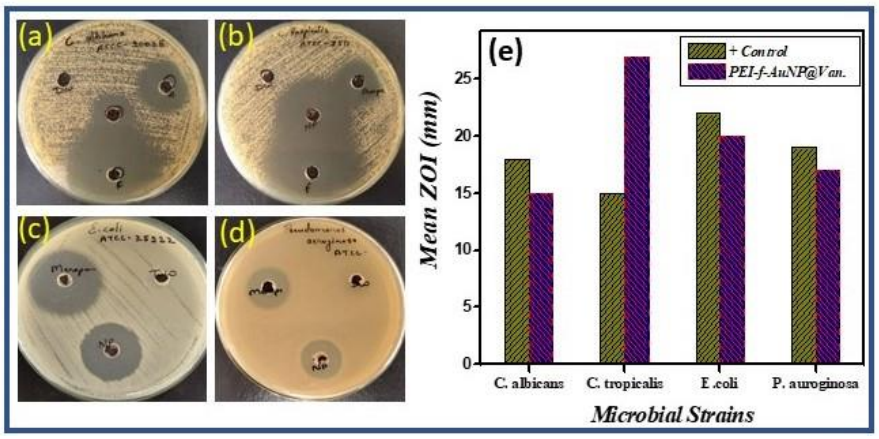

Figure 7.1 Representing the Agar well diffusion plates antimicrobial assessment of PEI-AuNP@Van and mean zone of Inhibition graph plot; (a) *C. albicans*, (b) *C. tropicalis*, (c) *E. coli*, (d) *P. aeruginosa* and (e) Mean zone inhibition graph.

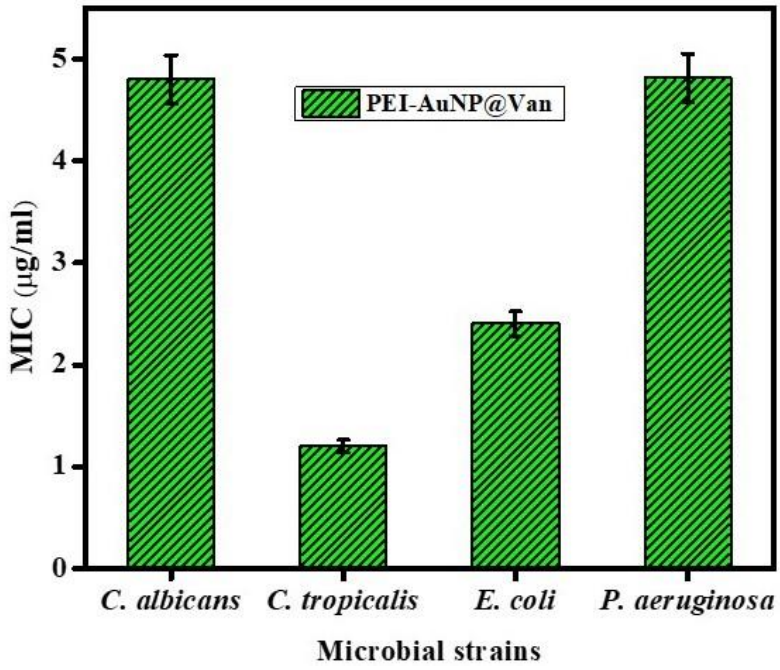

Figure 7.2 Representing the MIC values of vancomycin functionalized gold nanoparticles (PEI-AuNP@Van), against *C. albicans*, *C. tropicalis*, *E. coli* & *P. aeruginosa*.

7.3.3 Laser scanning super-resolution Confocal Microscopy (CLSM) Studies

It is obvious to assume that when PEI-AuNP@Van encounters microbial cells, it could bind to some specific location on the cell surface and lead to antimicrobial actions. Because PEI-AuNP@Van are fluorescent nanoparticles, they can be located upon specific excitation/emission ranges under confocal microscopy. As shown in Figure 7.3 (a-l), the PEI-AuNP@Van nanoparticles are adsorbed on a particular location on the microbial cell surfaces after 4 h of exposure. Interestingly, all PEI-AuNP@Van adsorbed cells had shown an intense blue signal, as shown in Figure. 7.3 and 7.4. Further, a live/dead assay was performed with the fluorescent dye Propidium iodide. The freshly prepared microbial strains were treated with respective MIC of PEI-AuNP@Van for 4h and stained with PI to visualize under confocal microscopy, as shown in Figure 7.5 (a-h). The recorded results confirmed that PEI-AuNP@Van potentially compromised the cell membrane of all treated microbial strains.

Further, the dead cell percentage was calculated using fluorescence-activated cell sorting after treatment of PEI-AuNP@Van by using PI dye, as shown in Figure 7.6 (a-d). It is demonstrated that 16.3 % population of *C. albicans*, 91.8 % of *C. tropicalis*, 12 % of *E. coli*, and 85.8 % of *P. aeruginosa* were dead after 4 h of treatment.

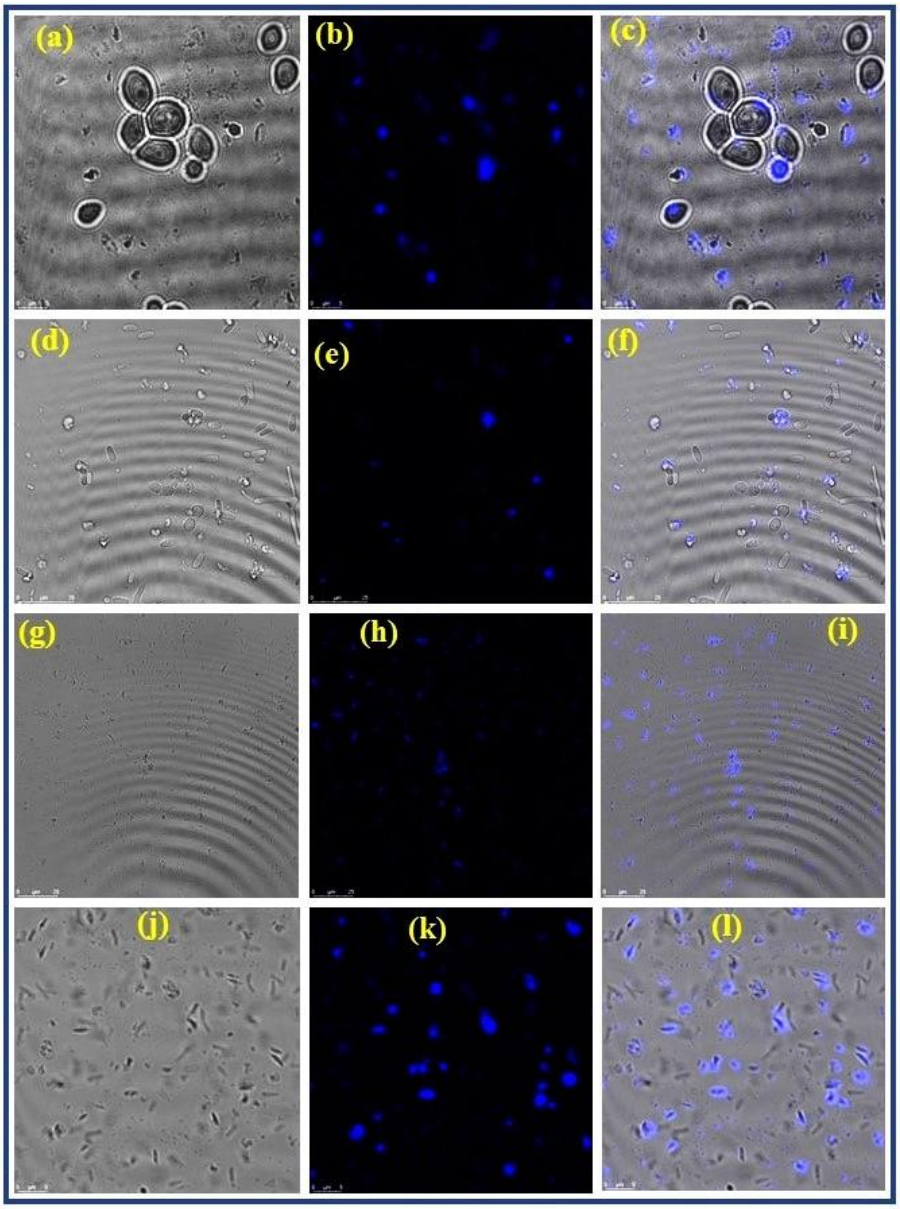

Figure 7.3 Representing localization of PEI-AuNP@Van around treated cells by using confocal microscopy along with DIC panels**.** (a) DIC panel of *C. albicans* (b) blue emission panel of PEI-AuNP@Van treated cells, (c) merged panel; (d) DIC panel of *C. tropicalis* (e)

blue emission panel of PEI-AuNP@Van treated cells, (f) merged panel; (g) DIC panel of *E. coli* (h) blue emission panel of PEI-AuNP@Van treated cells, (i) merged panel; (j) DIC panel of *P. aeruginosa* (k) blue emission panel of PEI-AuNP@Van treated cells and (l) merged panel.

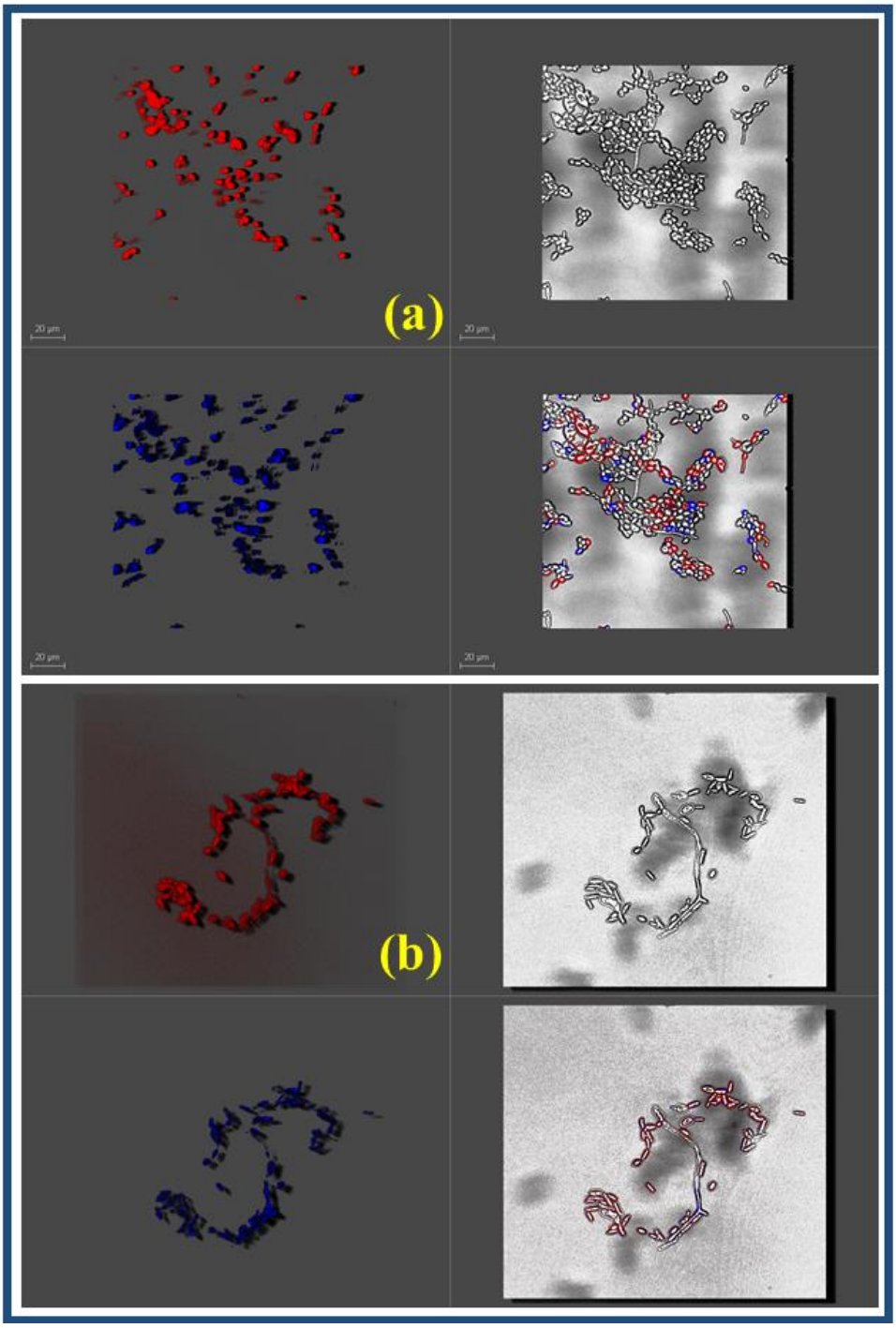

Figure 7.4 represents the intracellular localization of PEI-AuNP@Van nanoparticles inside the cell of *C. albicans* (a) and *C. tropicalis* (b) along with Red/blue panels and DIC panels.

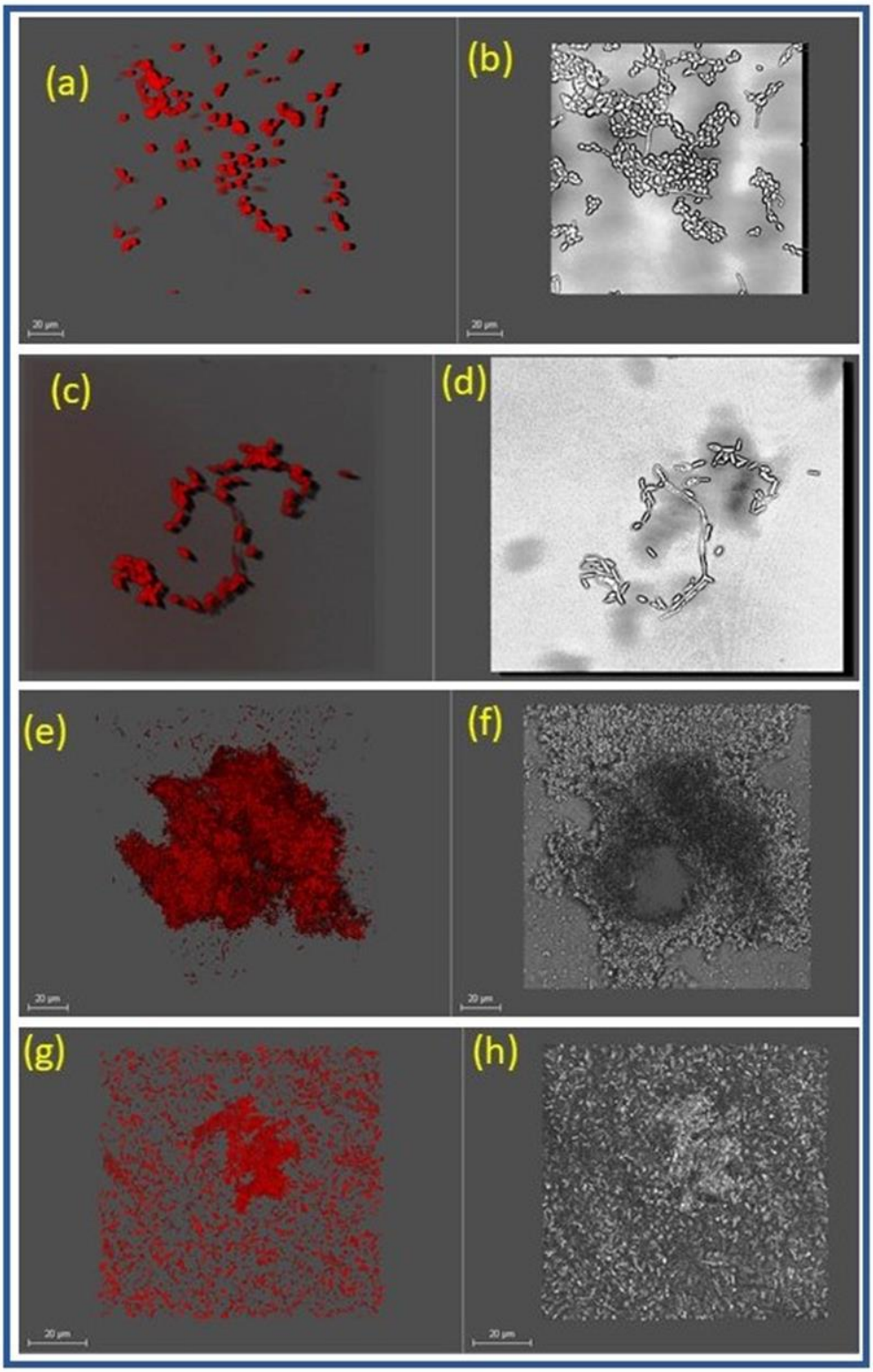

Figure 7.5 representing the confocal microscopy along with DIC images of PEI-AuNP@Van treated cells of *C. albicans* (a & b); *C. tropicalis* (c & d); *E. coli* (e &f) and *P. aeruginosa* (g & h).

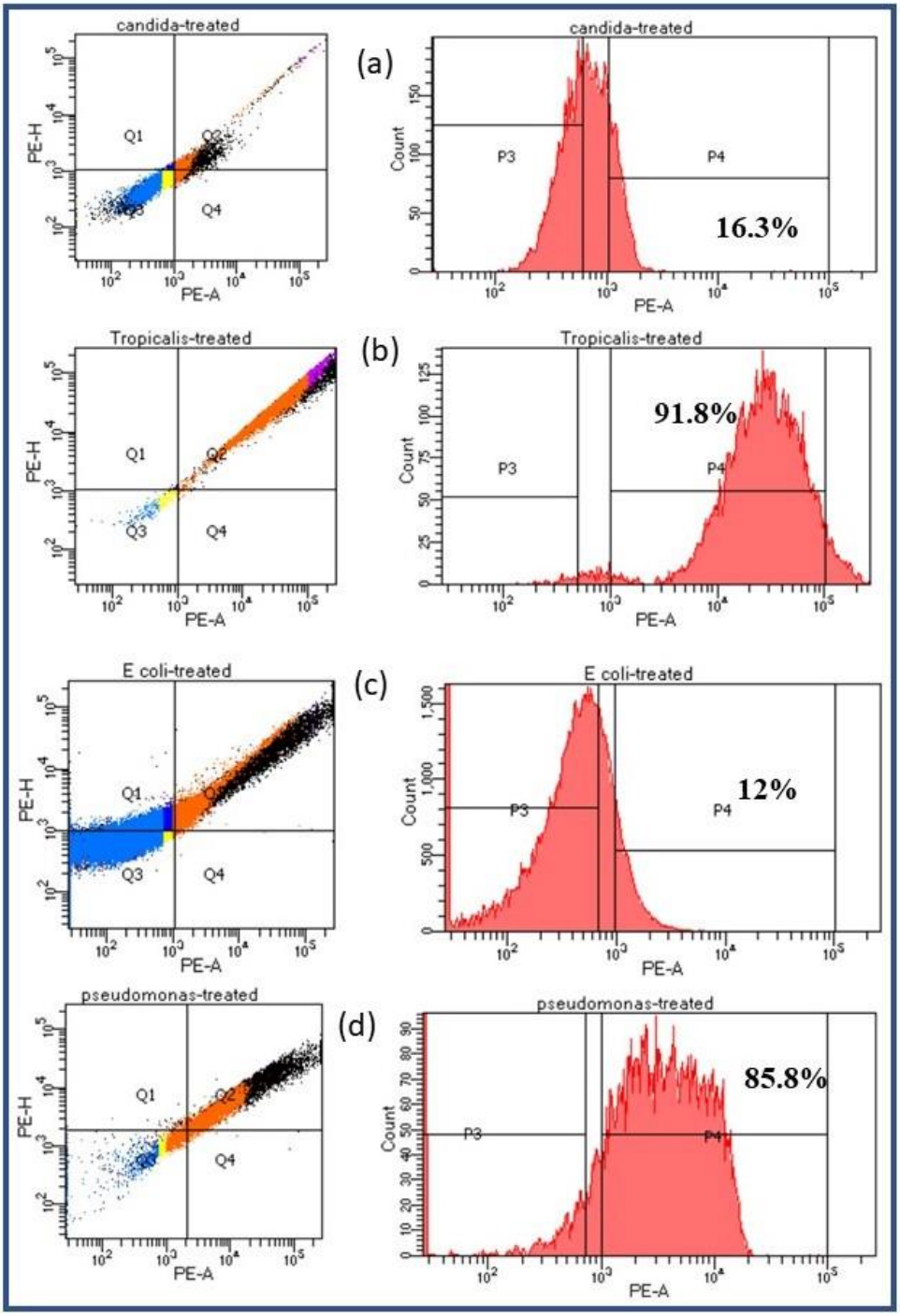

Figure 7.6 Representing histogram of cell Viability assay using PI as a probe against PEI-AuNP@Van treated microbial strains. (a) Showing untreated and treated histograms of *C.*

albicans; (b) Showing untreated and treated histograms of *C. tropicalis*; (c) Showing untreated and treated histograms of *E. coli* and (d) Showing untreated and treated histograms of *P. aeruginosa*.

7. 4 Antimicrobial mechanism

7.4.1 Endogenous ROS Generation Studies

The results of the MIC and viability assay were very encouraging. Then we evaluated ROS generation employing 2, 7-dichlorofluorescein diacetate (DCFH-DA) through flow cytometry after the treatment with PEI-AuNP@Van, (at respective MIC for each strain). We noticed significant differences in the ROS generation profiles of this PEI-AuNP@Van (Figure 7.7 a–d). Compared to the untreated control, treatment with PEI-AuNP@Van induced a substantial increase in the DCF fluorescence. The PEI-AuNP@Van treated *C. albicans*, *C. tropicalis*, *E. coli*, and *P. aeruginosa* exhibited only 11.38 %, 25.02%, 30.4 %, and 36.0 %, respectively, populations showing ROS generation as shown in Figure 7.7; however, untreated control cell population demonstrated negligible ROS generation. It was evident that, PEI-AuNP@Van induced high ROS generation against Gram-negative bacteria compared to *C. albicans* and *tropicalis*.

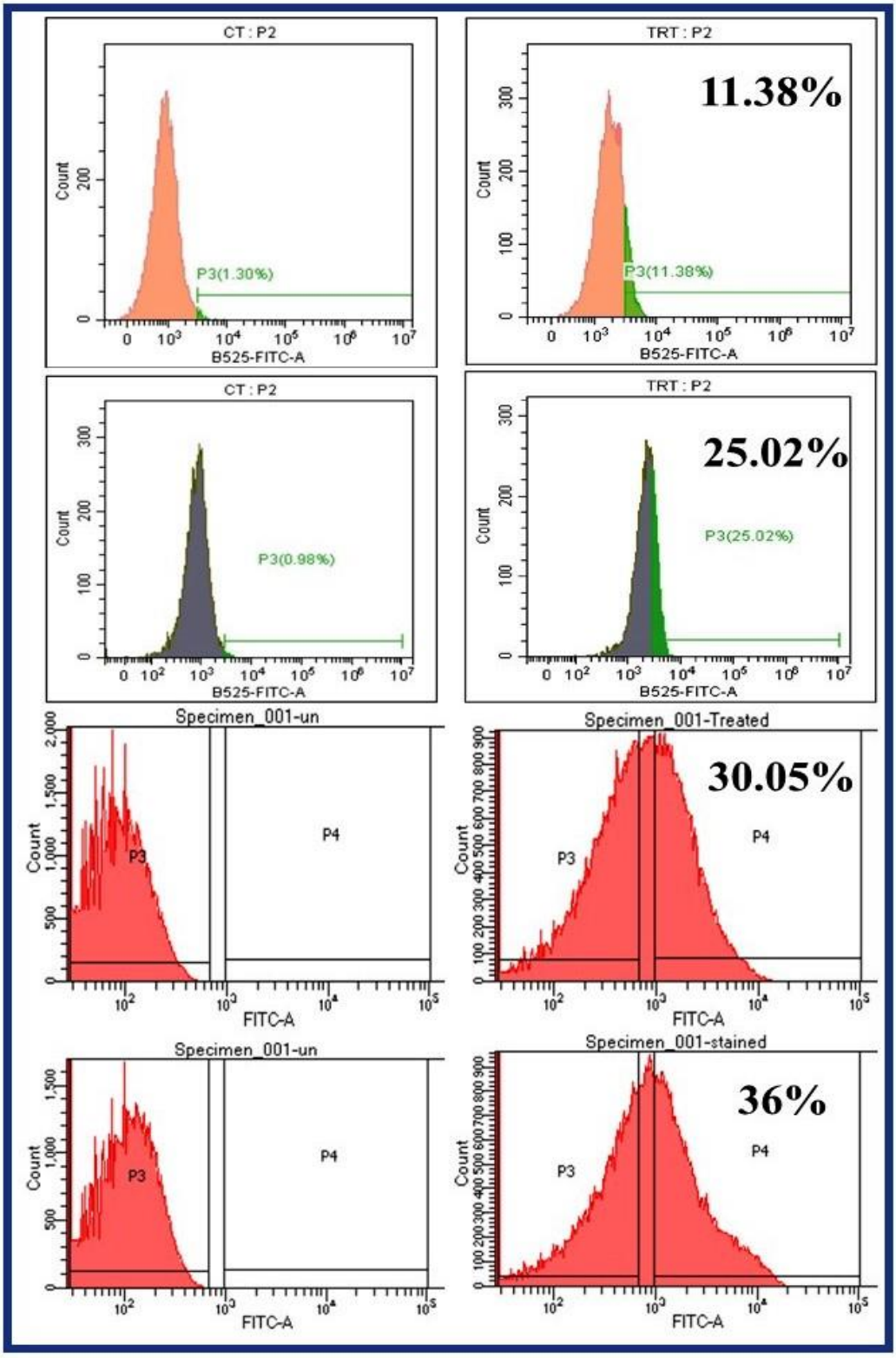

Figure 7.7 Representing histogram of endogenous ROS generation assay of PEI-AuNP@Van treated strains. (a) untreated control of *C. albicans*, (b) treated cells; (c) untreated control of

C. tropicalis, (d) treated cells; (e) untreated control of *E. coli*, (f) treated cells; (g) untreated control of *P. aeruginosa* and (h) treated cells

7.4.2 Phosphatidylcholine externalization studies

To determine whether PEI-AuNP@Van treated *C. albicans, C. tropicalis, E. coli*, and *P. aeruginosa* cells exhibit early apoptotic properties, Annexing V-FITC staining needs to be done with an intact membrane-impermeable dye such as PI and visualized under super-resolution confocal laser scanning microscopy. Phosphatidylserine is a negatively charged phospholipid known to translocate from the inner to the outer leaflet of the plasma membrane during the early stage of apoptosis. This early marker can be detected by Annexin V, which binds to externalized phosphatidylserine with high affinity in the presence of Ca^{2+} ions. Early apoptotic cells can only be stained with Annexin V-FITC in this double-staining method. In contrast, late apoptotic cells and necrotic cells are stained with PI through damaged membranes as well as stained with Annexin V-FITC. The result shows that all treated microbial strains exhibited early and late apoptotic properties except *C. albicans*, as demonstrated in Figure 7.8. Among all, *P. aeruginosa* has shown assertive delinquent apoptotic behavior, followed by *E. coli*, as shown in Figure 7.8 (j, k & l).

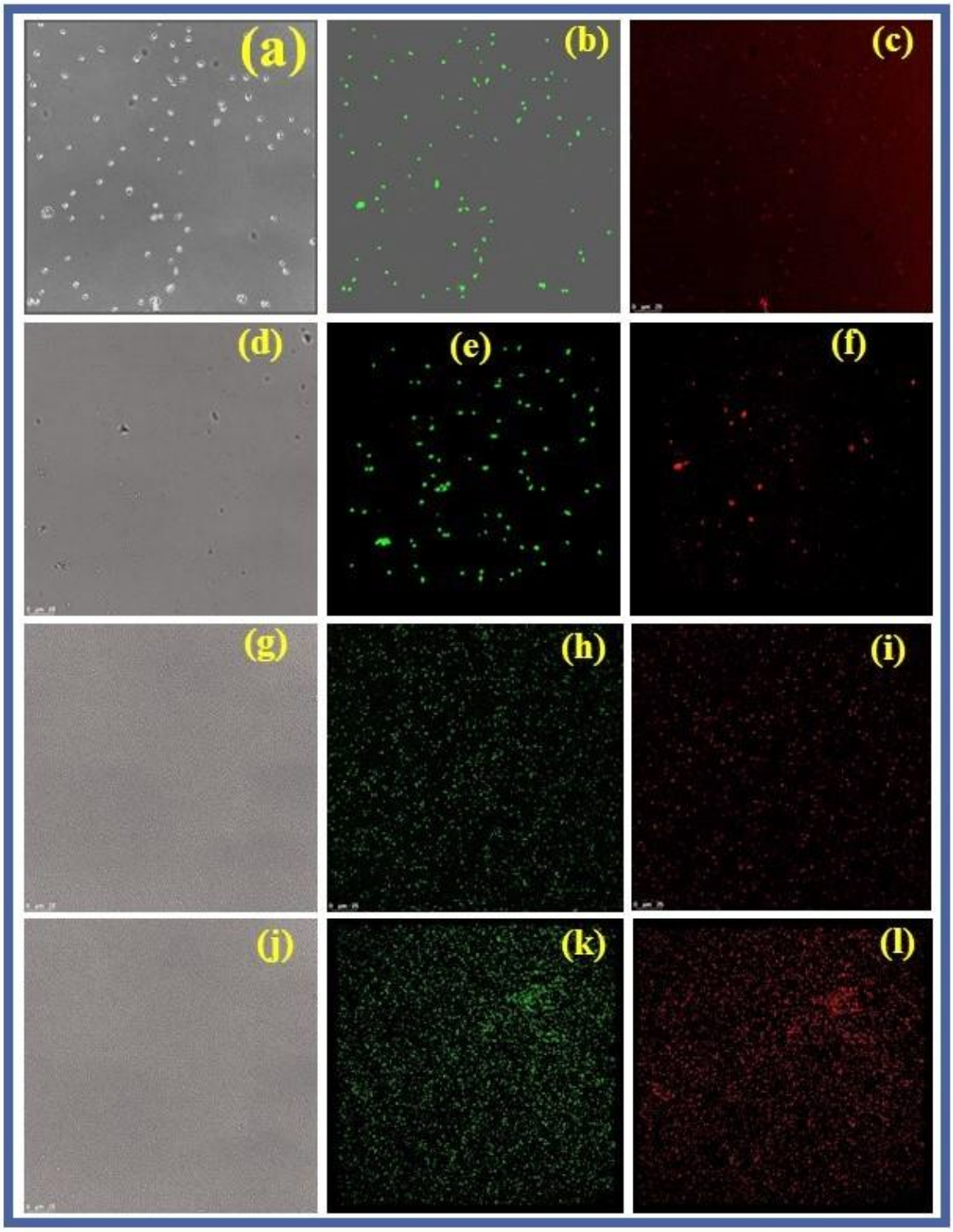

Figure 7.8 Representing Phosphatidylcholine externalization assay by using Annexin-V/PI system. (a) DIC panel of *C. albicans*, (b) green panel, (c) red panel; (d) DIC panel of *C.*

tropicalis, (e) green panel, (f) red panel; (g) DIC panel of *E. coli*, (h) green panel, (i) red panel; (j) DIC panel of *P. aeruginosa*, (k) green panel and (l) red panel.

7.4.3 Raman Spectroscopic Analysis

Raman spectrometry of *C. albicans*, *C. tropicalis*, *E. coli*, and *P. aeruginosa* was performed after treating PEI-AuNP@Van and untreated control. The recorded spectrum matched with previously characterized biomolecule fingerprints and structural assignments by different research groups (Zając et al., 2015; De Gelder et al., 2007; Freire et al., 2017; Xia et al., 2022; Raza et al., 2023; Witkowska et al., 2016; Hu et al., 2022; Sujith et al., 2009; Assmann et al., 2015; Neugebauer et al., 2006; Colniță et al., 2017) and concluded that there were significant architectural changes in PEI-AuNP@Van treated microbial cells compared to untreated cells.

7.4.4 Raman spectroscopic analysis of PEI-AuNP@Van and Amphotericin B treated *C. albicans and C. tropicalis*.

The Raman spectra of untreated PEI-AuNP@Van and Amphotericin B-treated *C. albicans* and *C. tropicalis* cells are illustrated in Figure 7.9 (a & b). The Raman spectrum of untreated *C. albicans and C. tropicalis* cells exhibited bands between wavenumber 480 to 1670 cm^{-1}, as shown in Figure 7.9 (a & b)**.** Similarly, Amphotericin B and PEI-AuNP@Van treated cells were recorded and demonstrated Raman bands between 480 to 1670 cm^{-1}. Based on the previous reports, these Raman bands can be assigned to particular macromolecules and their unique conditions. The untreated control cells Raman bands can be designated as 487 cm^{-1} (in-plane bending of CCO and torsion at COHO in Chitin, an integral part of *C. albicans and C. tropicalis* cell wall), 531 cm^{-1} (In-plane bending of (CCC), β(CCO), β(OCO) in Chitin) however same band observed at 539 cm^{-1}. Further, 726-735 cm^{-1} (Stretching in CO and ring deformation of glucosyl unit/Adenine and glycosides) are detected in both species of *Candida*, as shown in Figure 7.9 (a, b i). Similarly, bands 808-810 cm^{-1} can be assigned as

asymmetric stretching in OPO phosphodiester bond, and the band at 1040 cm^{-1} is C–C stretching (phospholipids carbohydrates, e.g., Chitin), C–N stretching. The band recorded at 1135 cm^{-1} could be =C–O–C= (unsaturated fatty acids of lipids) common in both species. The band at 1248 cm^{-1} in *C. tropicalis* can be assigned as Amide III (random); however, it is not detected in *C. albicans*. Further, both species' Raman bands at 1314 and 1323 cm^{-1} are Amide III of protein or CH deformation. A CH_2 deformation was recorded in both species at 1449 and 1452 cm^{-1}. Raman band at 1582 cm^{-1} in *C. tropicalis*, absent in *C. albicans*, can be assigned as NH2 deformations/Amide III protein. However, the band at 1663 cm^{-1} was typical in both species and fingerprint of Chitin. The above-assigned peaks are associated with *Candida* species cell walls composed of complex sugars and proteins such as mannoproteins, glucan, and Chitin.

Similarly, the Raman spectrum of Amphotericin B and PEI-AuNP@Van exposed cells were recorded and compared with untreated control cells to determine the mode of action and associated structural changes. The recorded Raman spectrum is demonstrated in Figure 7.9 (a, b; ii & iii). The interpreted differences between untreated control cells, Amphotericin B and PEI-AuNP@Van treated *C. albicans* and *C. tropicalis* cells were at 587 cm^{-1} (absent in *C. albicans*), 590 cm^{-1}, 676 cm^{-1}, 685 cm^{-1}, 852 cm^{-1} (absent in *C. albicans*), 914 cm^{-1}, 1125 cm^{-1}, 1162 cm^{-1}, 1214 cm^{-1} (absent in *C. albicans*), 1314 cm^{-1}, 1582 cm^{-1} (absent in *C. albicans*), 1602 cm^{-1} and 1653 cm^{-1} as shown in Figure 7.9 (a, b (ii & iii)) and Table 7. 1. These recorded spectral peaks can be tentatively assigned as in-plane bending of (CCC), β(CCO), β(OCO) in Chitin's glyosidic linkage (587 and 590 cm^{-1}); guanine and tyrosine at 676 cm^{-1}; in-plane bending of CCO in glucosyl unit (685 cm^{-1}, absent in *C. tropicalis*); twisting in (CH2), stretching (CC) glucosyl unit (852 cm^{-1}); stretching in CC bonds (914 cm-1 absent in *C. tropicalis*); C–O ring, aromatic amino acids in proteins (1162 cm^{-1}, absent in *C. tropicalis*) and Amide III (random), thymine (1214 cm^{-1}, absent in *C. albicans*).

7.4.5 Raman spectroscopic analysis of PEI-AuNP@Van treated cells of *E. coli* and *P. aeruginosa*

In contrast to *Candida* cell structure, Gram-negative bacterial cells are surrounded by a thin peptidoglycan cell wall surrounded by an outer membrane containing lipopolysaccharide. Raman spectroscopic analysis of PEI-AuNP@Van, Meropenem treated and untreated cells *E. coli* and *P. aeruginosa* recorded as shown in Figure 7.9 (c &d)**.** The untreated bacterial cells exhibited several weak and firm intensity peaks between wavenumbers 400-1660 cm^{-1}, as represented in Figure 7.9 (c, d (i))**.** In detail, the Raman spectrum band assignments can be made based on previously studies as 748 cm^{-1} in both strains (C–S (protein)/CH2 rocking/Adenine; peptidoglycan); 997 or 1002 cm^{-1} (in plane (CH), Phe, (CC) aromatic ring, ring-breathing (CC) polysaccharides); 1122 or 1127 cm^{-1} (Stretching (C–C) skeletal of acyl backbone in lipid); 1167 cm^{-1} (C–H in-plane bending mode of tyrosine, absent in *E. coli*); 1243 cm^{-1} (Asymmetric phosphate stretching modes; Amide III); 1311 cm^{-1} (CH2 wagging and twisting mode); 1329 cm^{-1} (COH (mono, oligosaccharide) Amide III, bend (CH), (OH) (polysaccharide) d (OH), in plane (CH2); 1341 cm^{-1} (amide III, Trp; dbend (CH), d (OH) (polysaccharide); 1392-1404 cm^{-1} (symm (CO2) alanine); 1450 cm^{-1} ((CH2) (fatty acid chains, phospholipids, amino side-chains of proteins); CH_3, CH_2, COH (mono or oligosaccharides); 1578-1585 cm^{-1} (νCOO−; C-C, N–H deformation; C–N stretching (amide II)) and 1658 cm^{-1} (Amide I). These demonstrated spectrum bands are fingerprint bonds of untreated cells**,** as shown in Figure 7.9 (c, d (i))**.**

Similarly, Meropenem and PEI-AuNP@Van treated *E. coli* and *P. aeruginosa* cells. Raman spectra were recorded and correlated with untreated control cells to interpret structural deformations. The recorded spectral bands differ slightly from untreated control cells in both strains, as shown in Figure 7.9 (c, d; ii & iii)**.** The peaks within the spectrum either disappeared or shifted in Meropenem and PEI-AuNP@Van treated cells. For example, peak at 534 cm^{-}

[1](COC glycosidic ring deformation; glucose-saccharide band; peptidoglycan); 848 cm^{-1} (Stretching (C-CH3) alanine ring-breathing (CC), Tyr, (COC) 1,4-glycosidic link; CO, CC, CH bending (oligosaccharides); 1506 (Amide II) and 1600 (Phe, Tyr) cm^{-1} was absent in untreated control cells in case of *E. coli* while, 637 (NCO) Tyrosine) and 1662 cm^{-1} (Amide I) were absent in *P. aeruginosa*. Most peaks are shifted to lower or higher wavenumbers, as shown in Figure 7.9 (c, d; ii & iii).

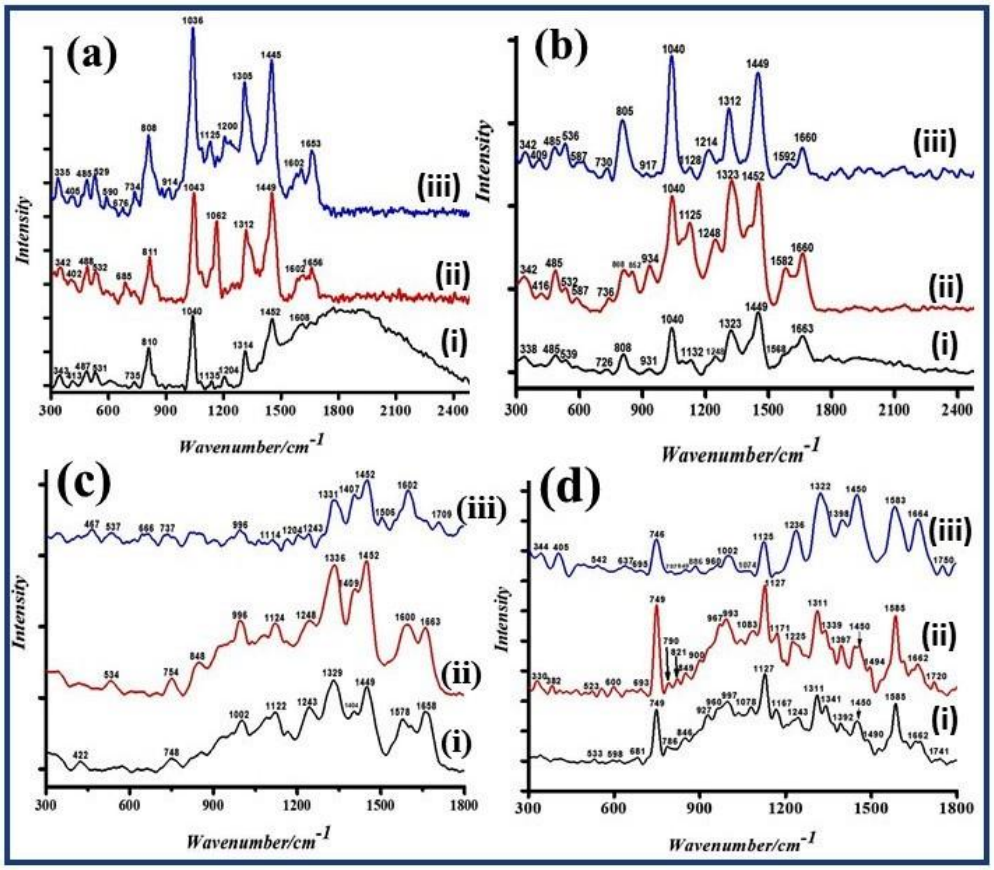

Figure. 7.9 Raman spectrometry of PEI-AuNP@Van exposed microbial cells along with positive control (Amphotericin B and Meropenem) and untreated cells. **(a)** ***C. albicans*** **(i)** Raman spectrum of untreated cell control; **(ii)** treated with amphotericin B and **(iii)** treated with PEI-AuNP@Van. **(b)** ***C. tropicalis*****, (i)** Untreated cell control*;* **(ii)** treated with Amphotericin B and **(iii)** treated with PEI-AuNP@Van. **(c)** ***E. coli*****, (i)** Untreated cell control*;* **(ii)** treated with Meropenem, and **(iii)** treated with PEI-AuNP@Van. **(d)** ***P. aeruginosa*****, (i)** Untreated cell control*;* **(ii)** treated with Meropenem, and **(iii)** treated with PEI-AuNP@Van.

7.4.6 TEM analysis

TEM analysis of PEI-AuNP@Van treated cells for 4 h. was performed to confirm the attachment of functionalized nanoparticles on the cell surface and any structural changes led by PEI-AuNP@Van. The results demonstrated that the surface interaction dynamics and mechanical impact of PEI-AuNP@Van against all strains were different, as shown in Figure 7. 10. Untreated cells of *C. albicans* were smooth and round shaped, while PEI-AuNP@Van treated cells appeared rough and cracked with loss of function, as demonstrated in Figure 7. 10 (a & e). In the case of *C. tropicalis* and *E. coli*, cells were utterly fractured as compared to untreated cells, as shown in Figure 7.10 (b, f, c & g). Figure 7. 10 (d & h) represents the control and treated cells of *P. aeruginosa*, respectively. Here, the functionalized nanoparticles seem to be attached to a specific location on the bacterial surface but not uniformly, indicating selective binding to some particular cell surface domain. However, no other structural changes were observed.

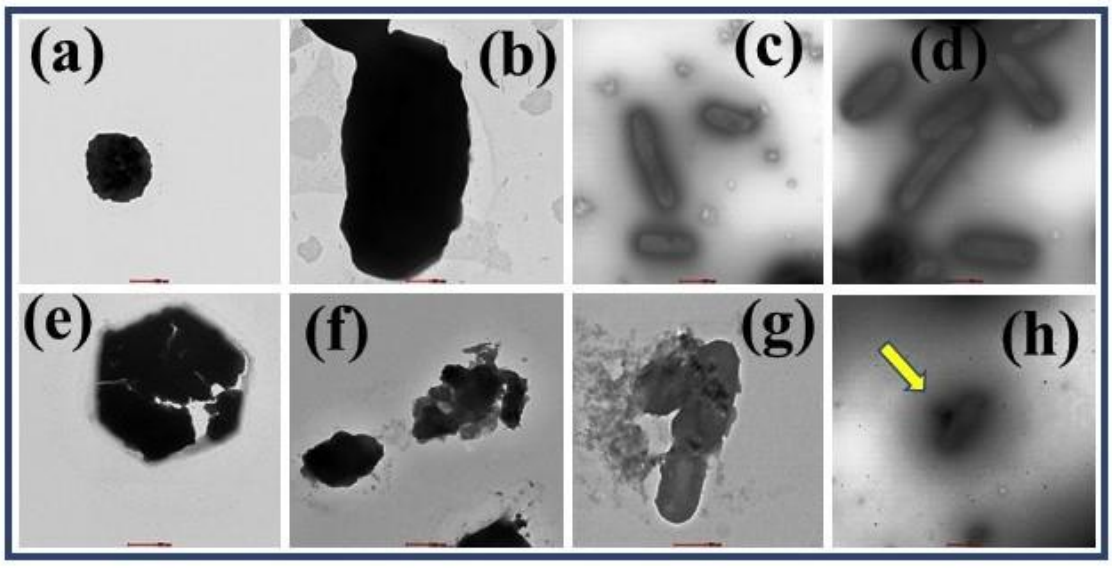

Figure 7.10 Representing TEM imaging of PEI-AuNP@Van treated cells of *C. albicans*, *C. tropicalis*, E. *coli*, and *P. aeruginosa*. (a) Untreated control of *C. albicans*, (e) PEI-AuNP@Van

treated; (b) untreated control of *C. tropicalis*, (f) PEI-AuNP@Van treated; (c) untreated control of *E. coli*, (g) PEI-AuNP@Van treated; (d) untreated control of *P. aeruginosa* and (h) PEI-AuNP@Van treated.

7.5 Discussion

The vancomycin-conjugated gold nanoparticles were synthesized and characterized using UV-Vis, TEM, DLS, XRD, and Zeta potential, as discussed in the previous chapter (Chapter 6). Except for applying PEI-AuNP@Van in sensing mercury, exploring the functionalized gold nanoparticles for effective delivery of vancomycin against Gram-negative bacteria such as *E. coli* and *P. aeruginosa* was rational.

7.5.1 Assessment of antimicrobial activity of PEI-AuNP@Van

Vancomycin is used as an antibacterial drug, mostly against Gram-positive bacteria, with a unique mode of action. It forms hydrogen bonds with the terminal D-alanyl-D-alanine moieties of the NAM/NAG-peptides, preventing the incorporation of the NAM/NAG-peptide subunits into the peptidoglycan matrix (Mühlberg et al., 2020). There is also evidence that vancomycin alters the permeability of the cell membrane and selectively inhibits ribonucleic acid synthesis (Watanakunakorn, 1984). Contrary to Gram-positive bacteria, the Gram-negative bacteria cell is covered with an extra layer of lipopolysaccharide that prevents the interaction of vancomycin with the peptidoglycans**.** However, the cell walls of yeasts, like those of *C. albicans* and *C. tropicalis*, comprise complex polysaccharides called Chitin and several proteins. *The Candida* cell wall is a two-layered structure. The main core of the cell wall is composed of a β-glucan-chitin skeleton, which is responsible for the strength and shape of the cell wall (Gow et al., 2017). The outer layer of the *Candida* cell wall is packed with mannoproteins that are glycosylphosphatidylinositol (GPI)-modified and cross-linked to β-1, 6-glucans. Therefore, it is obvious to investigate how PEI-AuNP@Van interacts with the microbial strain's surface and

associated death mechanism. Our previous study demonstrated that PEI-functionalized silver nanoparticles interact with the *C. albicans* and *A. baumannii* cell surface proteins and sporangiospores of *R. arrhizus* surface by electrostatic interaction and exerted antimicrobial activity via cell wall fracture (Tiwari et al., 2020; Tiwari et al., 2022)**.** Here, due to the cationic nature of PEI, it can bind to the anionic character of the cell surface along with vancomycin, which leads to vancomycin keeping close to the target macromolecule. Hence, the functionalization of vancomycin has shown potent antimicrobial activity against *C. albicans, C. tropicalis, E. coli*, and *P. aeruginosa*. Although peptidoglycans are absent in *Candida* cell walls, the vancomycin functionalized gold nanoparticles have shown potent antifungal activity against both *Candida* spp. However, the molecular mechanism is to be deciphered and needs an interdisciplinary approach.

Therefore, the antimicrobial activity of PEI-AuNP@Van was assessed against the two *Candida* app and two Gram-negative bacteria, namely, *C. albicans, C. tropicalis, E. coli*, and *P. aeruginosa*, along with MIC determination as shown in Figure 7.4 & 5**.** The PEI-AuNP@Van has demonstrated potent antimicrobial activity against all tested microbes with a MIC value ≤ 6 µg/ml. Notably, the conjugation of vancomycin to gold nanoparticles might have retained its antibacterial action. Our study agrees with previous findings that ceftriaxone, cefotaxime, and ampicillin maintain their antibacterial efficacy following conjugation to gold nanoparticles. Cefotaxime–AuNPs showed MIC values of 1.009 and 2.018 mg/L against drug-resistant *E. coli* and *K. pneumonia*, respectively (Shaikh et al., 2017). At the same time, the MICs of ceftriaxone–AuNPs against *E. coli, S. aureus*, and *K. pneumoniae* were determined as 1.39, 1.6, and 0.9 µg/mL, respectively (Shaikh et al., 2017). All these antibiotic-loaded gold nanoparticles showed enhanced efficacy than a pure antibiotic, which agrees with our findings, as shown in Figures 7.4 and 5**.** However, we did not identify any such report about the

antifungal activity of vancomycin-conjugated gold nanoparticles against the *Candida* spp. Although, PEI-AuNP@Van demonstrated good antifungal activity.

Further, based on the argument that PEI can anchor on microbial cell surfaces, we tried to visualize the binding of vancomycin-conjugated gold nanoparticles under confocal microscopy. As a result, shown in Figures 7.6 & 7.7**,** the functionalized gold nanoparticles were found to be adsorbed on the surface of the aforementioned microbial strains. However, in the case of *C. albicans* and *C. tropicalis*, the PEI-AuNP@Van seems to be localized intracellularly, as shown in Figure 7.7 (a & b). The cells were stained with PI after exposure to PEI-AuNP@Van and visualized under confocal microscopy on blue and red channels. The results demonstrated that membrane-compromised cells were filled with blue fluorescence, indicating the intracellular localization of PEI-AuNP@Van. This justifies structural differences and selective surface binding of PEI-AuNP@Van between *Candida* strains and Gram-negative bacterial cells.

Further, to ensure the membrane integrity of PEI-AuNP@Van treated fungal and bacterial cells along with death percent determination, PI staining was performed, followed by a combination of techniques such as confocal microscopy and flow cytometry employed as shown in Figure 7.8 & 7.9**.** Cellular and membrane integrity is one criterion distinguishing between viable and dead bacterial cells. Viable cells are assumed to have intact and tight cell membranes that cannot be penetrated by propidium iodide (PI). In contrast, dead cells are considered to have disrupted and broken membranes stained with PI. FCM is a rapid cell-by-cell multi-parameter analysis technique often used in combination with fluorescent labeling. Cells are analyzed at 100 to 1,000 per second as they are carried within a fast-flowing fluid stream that passes a focused light beam. The forward-angle light scatter (FSC), the side-angle light scatter (SSC), and the fluorescence at selected wavelengths are measured. The analyses are done on large populations of cells, typically 5,000 to 10,000. Subpopulations can be distinguished when they

differ in light scatter or fluorescence characteristics**.** Our results demonstrated that after 4 h of treatment with PEI-AuNP@Van, 16.3 %, 91.8 %, 12 %, and 85.8 % populations of *C. albicans, C. tropicalis, E coli*, and *P. aeruginosa*, respectively, had compromised membrane and considered dead. Compared to agar well diffusion, the viability assay results agreed with the zone of inhibition outcomes and suggested biocidal activity rather than biostatic property.

7.5.2 Antimicrobial Mechanism of PEI-AuNP@Van

To understand the mode of action of PEI-AuNP@Van against the strains mentioned above, we employed endogenous ROS generation assay, apoptosis assay, Raman spectroscopy, and TEM imaging of treated cells.

7.5.3 Intracellular ROS accumulation studies

ROS is generally produced during metabolic redox reactions and is a series of intermediate products formed in oxygen metabolism. Excessive ROS accumulation risks damage to cell membranes and intracellular biomolecules such as proteins and DNA, causing irreversible oxidative damage. This study monitored the PEI-AuNP@Van-induced ROS production in *C. albicans, C. tropicalis, E. coli*, and *P. aeruginosa* using H_2DCFDA dye and FACS analysis. 2′, 7′-Dichlorodihydrofluorescein diacetate (H_2DCFDA) is commonly used as a probe for detecting intracellular H_2O_2. The cell-permeable H_2DCFDA diffuses into cells and is deacetylated by cellular esterase to form 2′, 7′-dichlorodihydrofluorescein (H_2DCF). In the presence of H_2O_2, H_2DCF is rapidly oxidized to 2′, 7′-dichlorofluorescein (DCF), which is highly fluorescent, having excitation and emission wavelengths of 498 and 522 nm, respectively. The oxidation of H_2DCF to DCF is thought to be specific for H_2O_2, and recent evidence has shown that other ROS, such as hydroxyl radical, hydroperoxides, and peroxynitrite, can also oxidize H_2DCF. Therefore, PEI-AuNP@Van treated cells of the aforementioned microbial strains had demonstrated intracellular ROS accumulated in 11.38 %, 25.02 %, 30 %, and 36.30 % cell populations of *C. albicans, C. tropicalis, E. coli*, and *P.*

aeruginosa respectively after 4 h. of exposure as shown in Figure 7.8**.** When the obtained results were validated with percent dead cells, as shown in Figure 7.7, it was in good agreement.

7.5.4 Raman Spectroscopic Studies

Raman spectroscopy is an ideal tool for analyzing the spatial structure of biological macromolecules. A Raman spectrum is an emission spectrum generated by high-frequency, inelastic scattering of light resulting from the response of a molecule to incident rays. Every macromolecule has a unique fingerprint Raman spectrum. When normal cells interact with engineered nanoparticles, macromolecules' structural conformation and relative content constitute a cell change. For example, the phosphate backbone of nucleic acids differs, hydrogen bonds between protein molecules are damaged, and the lateral stacking force of lipid molecules is reduced. These changes contribute to corresponding unique changes in the Raman spectra of the molecules in exposed cells. The yeast cells constitute a complex outer cell wall having Chitin, mannoproteins, and several sensory and architectural proteins. However, gram-negative bacterial cells exhibit an outer layer of complex lipopolysaccharides called the LPS layer, followed by peptidoglycan sheets and some surrounding proteins. Thus, analysis of Raman spectra can reveal structural and spatial changes in microbial cell walls after the exposure of functionalized nanoparticles. Therefore, Raman spectrometry performed for amphotericin B, Meropenem, and PEI-AuNP@Van treated aforementioned fungal and Gram-negative bacterial cells along with respective untreated control as shown in Figure 7.11**.** The results suggest that the action of PEI-AuNP@Van against the bacteria and fungus was different.

In the case of *C. albicans*, Raman peaks at 590 cm^{-1} (In-plane bending of (CCC), β(CCO), β(OCO) in Chitin (glycosidic linkage), 676 cm^{-1} (Guanine, tyrosine), 914 (Stretching in CC bonds), 1125 cm^{-1} (C–O–C= (unsaturated fatty acids in lipids), 1314 cm^{-1} (Amide III random), 1602 cm^{-1} (Guanine) and 1653 cm^{-1} (Chitin) as indicated in Figure 7.11 (a; iii). These peaks

are significant to PEI-AuNP@Van treated *C. albicans* and suggest the possible supramolecular changes in N-acetyl-d-glucosamine linked through a β-(1, 4)-glycosidic bond of cell wall. Further, the peak at 1135 cm^{-1} in untreated control shifted (shifting of peaks towards lower or higher wavenumber is related to the chemical bond length of molecules) to 1125 cm^{-1}, suggesting disintegration of the unsaturated lipid chain in the membrane. The detection of guanine and tyrosine (peaks at 676 & 1602 cm^{-1}) in treated cells indicated cellular fracture after treatment. These molecular changes were further validated by ROS accumulation, and TEM analysis that suggested PEI-AuNP@Van induces excessive ROS generation that damaged cell walls and membranes as visualized in TEM images as shown in Figure 7. 11 (a & e).

Similarly, Raman spectrometry of *C. tropicalis* demonstrated several molecular changes after PEI-AuNP@Van exposure. For example, shifting in peak at 535 cm^{-1} to 526 cm^{-1} suggested in-plane bending in (CCC), β (CCO), β (OCO) of chitin component and at 587 cm^{-1} in-plane bending in glycosidic linkage as shown in Figure 7. 11 (b; iii). The peak at wavenumber 852 cm^{-1} indicated twisting in (CH_2), stretching (CC) glucosyl unit of Chitin, and peak at 931cm^{-1} in untreated control cells shifted to lower wave number (917 cm^{-1}) after exposure, possibly due to C=C deformation and stretching in C–N bonds of lipids. Further, Amide III (protein), C–H deformation, and NH_2 deformations/Amide III protein (at 1312 & 1592 cm^{-1}) indicated damage to protein structure. Overall, the observed molecular changes are associated with structural damage of the cell wall and cell membrane, suggesting the mode of action of PEI-AuNP@Van is like *C. albicans*, which means excessive ROS accumulation in cells leads to the cellular collapse as demonstrated in TEM images **(**Figure 7.11; b & f**).**

The cellular composition and structure of Gram-negative bacteria *E. coli* and *P. aeruginosa* are fundamentally similar; however, at genus and strain levels, several molecular differences are there. Representative Raman spectra of *E. coli* and *P. aeruginosa* are shown in Figure 7. 9 (c & d). Raman spectra of *E. coli* untreated control (Figure 7.9**, c;** (i) Meropenem

treated **(ii)** and **(iii)** PEI-AuNP@Van treated cells exhibited peaks in region 530-550 cm^{-1}, typically COC glycosidic ring deformation of peptidoglycan and 848 cm^{-1} are Stretching in C-CH_3, alanine ring-breathing in C-C, tyrosine, (COC) 1,4-glycosidic link; CO, CC, CH bending. Peptidoglycan sheets are composed of alternating N-acetylglucosamine (NAG) and N-acetylmuramic acid (NAM) residues connected by β-(1, 4)-glycosidic bonds and cross-linked with short polypeptide chains; hence, structural deformation in glycosidic linkage can leads to breakage of cell wall and also endorsing the mode of action of vancomycin. Further, significant spectral changes are recorded as the peak at 1122 cm^{-1} in untreated cell spectrum shifted to lower wavenumber at 1114 cm^{-1} in PEI-AuNP@Van treated cells are typically due to Stretching (C–C) skeletal of acyl backbone in lipid; CN and CC stretching in carbohydrates. These molecular changes further correlated with TEM imaging and endorsed the finding that peptidoglycan sheet cells are fractured due to molecular changes, as shown in Figure 7.10 (c & g).

On the other hand, *P. aeruginosa* did not exhibit any significant vibrational changes between untreated control cells and PEI-AuNP@Van treated cells, as represented in Figure 7.9 **(d).** Few vibrational peaks could be considerable; for example- the peak at 533 cm^{-1} in untreated spectrum shifted to 542 cm^{-1} after exposure, representing COC glycosidic ring deformation; glucose-saccharide band; peptidoglycan and peak at 786 cm^{-1} shifted to 797 cm^{-1} exhibited stretching in phosphodiester linkage in lipids. Overall, after validation with TEM imaging, no cellular fracture was observed; however, PEI-AuNP@Van nanoparticles were adsorbed on the cells' surface, as shown in Figure 7.10 (d & h**).**

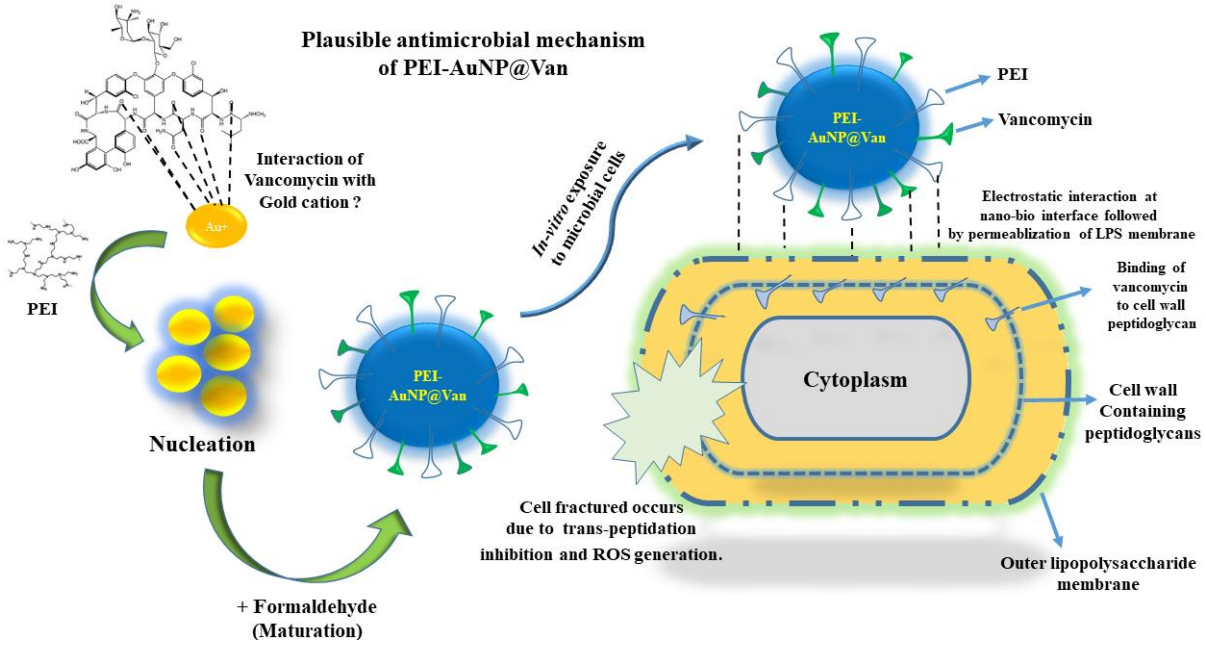

Figure 7.11 Possible mode of action of PEI-AuNP@Van against gram-negative *E. coli* and *P. aeruginosa*.

7.6 Conclusion:

In conclusion, we synthesized the vancomycin functionalized PEI stabilized gold nanoparticles to explore antimicrobial activity against *C. albicans*, *C. tropicalis*, *E. coli*, and *P. aeruginosa*. The synthesized PEI-AuNP@Van have shown potent antimicrobial activity within 4 hours of treatment against all tested microbial strains with a lower MIC value as *C. albicans* (4.8 µg/ml), *C. tropicalis* (1.2 µg/ml), *E. coli* (2.5 µg/ml), and *P. aeruginosa* (4.81 µg/ml) respectively. Further, PEI-AuNP@Van treated cells of C. albicans and C. tropicalis have demonstrated blue emission after laser irradiation suggested, PEI-AuNP@Van were internalized inside cells. Unlike *Candida* spp., PEI-AuNP@Van gets adsorbed on the surface of *E. coli* and *P. aeruginosa* cells. Viability assay confirmed that 16.3 % of *C. albicans*, 91.8 % of *C. tropicalis*, 12 % of *E. coli*, and 85.8 % of the *P. aeruginosa* population were killed after 4 h of treatment. Antifungal mechanism demonstrated that PEI-AuNP@Van exposed cells of strains mentioned

above get accumulated endogenous ROS in *C. albicans*, *C. tropicalis*, *E. coli*, and *P. aeruginosa* as 11.38 %, 25.02%, 30.4 %, and 36.0 %, respectively. Accordingly, the Phosphatidylcholine externalization assay confirmed apoptosis-like behavior in all PEI-exposed strains. Raman spectroscopy and TEM analysis confirmed the mode of action of PEI-AuNP@Van against all exposed strains. *C. albicans* and *C. tropicalis* killing was associated with ROS-induced apoptosis and cell wall damage; however, *E. coli* and *P. aeruginosa* exhibited ROS-induced apoptosis and deterioration in peptidoglycan sheet by vancomycin. Overall, designing and exploring anti-bacterial drugs against fungi and drug-resistant bacterial strains using an efficient delivery system like gold nanoparticles could be a potential weapon to tackle emerging antimicrobial drug resistance.

Table 7.1. Raman band assignments of PEI-AuNP@Van treated microbial strains (- indicating absence of Raman peak and + representing presence of Raman peak)

		C. albicans		
Wavenumber (cm^{-1})	**Untreated**	**Amphotericin B treated**	**PEI-AuNP@Van treated**	**Assignments**
487	+	+ (488)	+ (485)	In-plane bending in COC of galactomannan & Chitin
531	+	+ (532)	+ (529)	In-plane bending of (CCC), β(CCO), β(OCO) in Chitin
590	-	-	+	In-plane bending of (CCC), β(CCO), β(OCO) in Chitin (glyosidic linkage)
676	-	-	+	Guanine, tyrosine
685	-	+	-	In-plane bending of CCO in glucosyl unit

735	+	-	+	Adenine and glycosides
810	+	+	+	antisymmetric stretching in OPO phosphodiester
914	-	-	+	Stretching in CC bonds
1040	+	+	+	C–C stretching (phospholipids carbohydrates, e.g. chitin), C–N stretching
1125	+ (1135)	-	+	=C–O–C= (unsaturated fatty acids in Lipids).
1162	-	+	-	C–O ring, aromatic amino acids in Proteins
1200	+	-	+ (1204)	β(OH), β(CH)
1314	+	+ (1312)	+ (1305)	Amide III random
1452	+	+ (1449)	+ (1445)	CH_2 deformation
1602	-	+	+	Guanine
1608	+	-	-	Uracil
1653	-	+	+ (1656)	Chitin

C. tropicalis

485	+	+	+	In-plane bending in COC of galactomannan & Chitin
539	+	+ (532)	+ (526)	In-plane bending of (CCC), β(CCO), β(OCO) in Chitin
587	-	+	+	In-plane bending in glycosidic linkage
726	+	+(736)	+(730)	Stretching in CO and ring deformation of glucosyl unit/Adenine and glycosides
808	+	+	+(805)	antisymmetric stretching in OPO phosphodiester of nucleotides
852	-	-	+	Twisting in (CH2), stretching (CC) (glucosyl unit
931	+	+(934)	+(917)	C=C deformation, C–N stretching
1040	+	+	+	C–C stretching (phospholipids carbohydrates, e.g. chitin), C–N stretching

1132	+	+ (1125)	+ (1128)	=C–O–C= (unsaturated fatty acids in lipids), stretching in CO of galactomannan
1214	-	-	+	Amide III (random), thymine
1248	+	+	-	Amide III (random)
1323	+	+	+ (1312)	Amide III (protein), C–H deformation
1449	+	+ (1452)	1449	CH2 deformation
1582	-	+	+ (1592)	NH_2 deformations/Amide III protein
1663	+	+ (1660)	+ (1660)	Chitin
		E. coli		
422	+	-	-	ND
534	-	+	+ (537)	COC glycosidic ring deformation; glucose-saccharide band; peptidoglycan
748	+	+ (754)	+ (737)	Ring breathing DNA
848	-	+	+	Stretching (C-CH_3) alanine ring-breathing (CC), Tyr, (COC) 1,4-glycosidic

				link; CO, CC, CH bending (oligosaccharides, trehalose)
1002	+	+ (996)	+ (996)	in-plane (CH), Phe, (CC) aromatic ring, ring-breathing (CC) polysaccharides
1122	+	+ (1124)	+ (1114)	Stretching (C–C) skeletal of acyl backbone in lipid
1243	+	+ (1248)	+	Asymmetric phosphate [PO_2^- (asymmetric)] stretching modes; Amide III
1329	+	+ (1336)	+ (1331)	COH (mono-, oligosaccharide) amide III, bend(CH), (OH) (polysaccharide)
				d(OH), in plane (CH_2)
1404	+	+	+	Stretching (CO_2) (a-amino acids)
1449	+	+	+	(CH_2) (fatty acid chains, phospholipids, amino side-chains

				of proteins);CH_3, CH_2, COH (mono-, oligo saccharides
1506	-	-	+	Amide II
1578	+	-	-	νCOO; C-C, N–H deformation; C–N stretching (amide II)
1600	-	+	+	Phe, Tyr
1658	+	+ (1663)	-	amide I
1702	-	-	+	ND
		P. aeruginosa		
533	+	+ (523)	+(542)	COC glycosidic ring deformation; glucose-saccharide band; peptidoglycan
598	+	+ (600)	-	(CCC) ring deformation (monosubstituted benzenes)
637	-	-	+	(NCO) Tyr
681	+	+ (693)	+ (695)	ND
749	+	+	+	C–S (protein)/CH_2 rocking/adenine; peptidoglycan
786	+	+ (790)	+ (797)	Phosphodiester stretching

846	+	+ (849)	+ (849)	Stretching (C-CH_3) alanine ring-breathing (CC), Tyr, (COC) 1,4-glycosidic link; CO, CC, CH bending (oligosaccharides, trehalose
997	+	+	+	in-plane (CH), Phe, (CC) aromatic ring, ring-breathing (CC) polysaccharides
1078	+	+	+	Stretching (0=P-O-)DNA
1127	+	+	+	Stretching (C–C) skeletal of acyl backbone in lipid
1167	+	+	-	C–H in-plane bending mode of tyrosine
1243	+	+ (1225)	+ (1236)	Asymmetric phosphate [PO_2 − (asymmetric)] stretching modes; Amide III
1311	+	+	+ (1322)	CH_2 wagging and twisting mode
1341	+	+	-	amide III, Trp; bend in (CH), d(OH) (polysaccharide

1392	+	+ (1397)	+ (1398)	Symm. (CO2) alanine
1450	+	+	+	(CH_2) (fatty acid chains, phospholipids, amino side-chains
1585	+	+	+	C-C, N–H deformation; C–N stretching (amide II)
1662	+	+	+	Amide I